Brazilian Journal
of Chemical
Engineering

ISSN 0104-6632
Printed in Brazil
www.abeq.org.br/bjche

Vol. 36, No. 02, pp. 669 - 680, April - June, 2019
dx.doi.org/10.1590/0104-6632.20190362s20180215

REMOVAL OF TRIBUTYL PHOSPHATE FROM AQUEOUS SOLUTIONS BY TiO_2 HETEROGENEOUS PHOTOCATALYSIS SUPPORTED OVER A NEW METAL PLATE WITH KINETIC STUDY

Otidene R. S. da Rocha[1*], Joyce E. Oliveira[1], Luciano C. Almeida[1], Tulio D. da Silva[2], Josivan P. da Silva[1], Welenilton J. Nascimento Júnior[1] and Renato F. Dantas[3]

[1] Universidade Federal de Pernambuco, Departamento de Engenharia Química, Recife, PE, Brasil.
E-mail: otidene.rocha@ufpe.br - ORCID: 0000-0001-5216-1752
[2] Centro de Tecnologias Estratégicas do Nordeste, Recife, PE, Brasil.
[3] Universidade Estadual de Campinas, Faculdade de Tecnologia, Limeira, SP, Brasil.

(Submitted: May 21, 2018 ; Revised: August 7, 2018 ; Accepted: September 3, 2018)

Abstract - The aim of this investigation was to study the degradation of tributyl phosphate (TBP) in aqueous solution by heterogeneous photocatalysis (UV-C/TiO_2). To perform the investigation, aqueous solutions containing the contaminant were exposed to UV radiation in the absence or presence of TiO_2 in suspension or supported on a Fe-Cr metal alloy plate. TBP analyses before and after the treatment were performed by Ultra-Performance Liquid Chromatography (UPLC) in order to quantify the contaminant degradation. The results showed that the TiO_2 photocatalytic system was able to remove TBP from the solution and the formation of some by-products was observed. TiO_2 photocatalytic systems were able to reduce acute toxicity in an *Artemia Salina* bioassay according to the increase in LC_{50} from 10.2 ± 0.5%(v/v) to 16.9 ± 0.6 %(v/v) for the immobilized system and to levels which were not possible to detect by the applied method any more for the suspension system.
Keywords: Advanced oxidation; Wastewater treatment; ANN; Photocatalysis; Toxicity bioassay.

INTRODUCTION

The development of analytical methods has led to the detection and quantification of Emerging Contaminants (ECs) in the environment. The study of these contaminants has become an object of interest of large organizations such as the World Health Organization (WHO) and the European Commission (Estévez et al., 2012). ECs are defined as chemicals whose presence has recently been detected in several environments and their ecological and health effects are causing increasing concern around the world. They include pharmaceuticals, personal care products, detergents, food additives and pesticides, among others (Focazio et al., 2008; Estévez et al., 2012; De la Cruz et al., 2013; Giannakis et al., 2015).

Among the ECs, the Organophosphate Flame Retardants (OPFRs) are becoming important in the last decades. The concern comes from their large use in several types of materials since they are chemicals added to the material to prevent combustion and retarding the spread of fire after ignition. Most flame retardants tend to be leached from the material they are fixed in because they are just physically bonded to the material in which they are used and can be easily released in the environment (de Wit et al., 2010; Krivoshiev et al., 2015). OPFRs are formed by organic esters with phosphorus bonds to one or more oxygen

* Corresponding author: Otidene R. S. da Rocha - E-mail: otidene.rocha@ufpe.br

molecules. They are toxic and persistent, causing negative effects to the environment and human health (Liu et al., 2013a; Cristale et al., 2016). In addition, some of them have neurotoxic and carcinogenic characteristics (Flaskos, 2012).

The conventional treatment methods such as biological oxidation are inefficient in the removal of OPFRs from effluents due to the bioaccumulative and refractory nature of these compounds. In this sense, the search for new technologies has been encouraged, but there is still a lack of studies on the treatment of these class of pollutants in literature. Among the advanced methods to treat water, advanced oxidation processes (AOPs) have been widely used to degrade organic and inorganic contaminants, as well as to improve the biodegradability of industrial wastewater (Klavarioti et al., 2009; Matilainen and Sillanpää, 2010; Oller et al., 2011). They are based on the generation of highly reactive radicals that promote degradation at elevated rates non-selectively.

TiO_2 was proven to be the most suitable semiconductor to perform the heterogeneous photocatalytic degradation of organic compounds due to its properties, such as high photocatalytic activity, lack of toxicity and low cost (Cheng et al., 2016). The main challenge in heterogeneous systems is the further separation of the photocatalyst from the media at the end of the treatment. For this purpose, many catalysts are supported over other solid surfaces in order to ease the catalyst recovery. Despite the expenses of the immobilization and the minimization of the efficiency when compared to application in powder form, the costs associated with sedimentation, filtration, additional time and energy are remarkably reduced (Shen et al., 2016; Jung et al., 2017). Thus, TiO_2 on a substrate is highly desirable in order to recover easily the substance and many different materials have been applied in that sense. Nanotube arrays, for example, represent an enhancement in light harvesting and surface area, but are also associated to complexity and high cost (Shen et al., 2016). Clay minerals and modified clay minerals are the subject of great attention as well because some of them can induce oxygen vacancies improving photocatalytic performance (Wang et al., 2016). Many researchers have focused on immobilizing TiO_2 on metallic supports such as Ag, Pt, and Au (Dai et al., 2017; Hsieh et al., 2017). However, in some cases they can deactivate the catalyst during the reaction time and generate some undesirable intermediates in the surface of the support. Bimetallic catalysts can present more favorable properties related to deactivation and efficiency than monometallic (State et al., 2017); this is the reason why an alloy was used as a support.

The characterization of solid surfaces when immobilized with thin layers of other materials is traditionally done by Energy Dispersive Spectrometry coupled with Scanning Electronic Microscopy (SEM-EDS) and X-Ray Diffraction (XRD). SEM-EDS requires flat-polished specimens and, along with XRD, is able to provide microstructure features and composition of the bulk material through a mapping of the surface in high resolution (Sagar et al., 2016; Borges et al., 2017). XRD is also able to identify any impurities present on the surface (Ouyang et al., 2017).

The kinetic study of the oxidation processes of complex organic molecule treatments is often challenging to totally comprehend due to the lack of knowledge about all the possible reactions steps. A statistical and mathematical analysis is necessary to create an effective predictive model according to Sanusi et al. (2016).

Artificial Neural Networks (ANN) have been applied to solve a great variety of tasks which are difficult to solve by computational programs based on more simple rules. They can be used as mathematical tools for non-linear problems even in multi-dimensional approaches, which make them useful to analyse compound degradation patterns in complex chemical processes, as evidenced by Willumeit et al. (2013). A predictive model that describes TBP degradation can be achieved by fitting the data to several variations in response executed by ANN.

AOPs are extensively proven to modify the organic matter to form simpler compounds. However, byproducts with higher toxicity than the parental compounds can be formed as a result of oxidation. Thus, an acute toxicity evaluation is important to estimate ecological risks posed by the discharge of more toxic byproducts (Karci et al., 2013). In the last decades, several invertebrates have been used to investigate their sensitivity to possible toxic organic pollutants such as pesticides, pharmaceuticals, hormones, etc. *Artemia salina* (brine shrimps), one of the most common organism used in toxicity assessments, are branchiopod crustaceans capable of growing at low O_2 concentrations and high saline conditions. They present many advantages such as speed (28-72 hours from egg hatching to the end of the assay), low cost, high efficiency, easy manipulation and the assay can be carried out in small recipients (Lo Nostro et al., 2015; El Fels et al., 2016; Libralato et al., 2016).

The aims of this work included immobilizing TiO_2 over a Fe-Cr metal alloy plate, as well as characterizing the metallic support, studying comparatively the degradation of TBP by direct UV-C photolysis and a UV-C/TiO_2 photocatalytic system (supported and in suspension), monitoring TBP degradation through chromatographic analysis. A toxicity assessment using *Artemia salina* was carried out in order to verify the environmental acute toxicity caused by the TBP degradation by AOP treatment through the calculation of the lethal concentration (LC_{50}), the relationship

between the concentration of a chemical compound and the toxic effect caused by it in the tested organism.

MATERIALS AND METHODS

TBP Degradation Experiments

TBP samples were prepared with distilled water at a concentration of 100 μg.L^{-1}. The chemical was purchased from Sigma-Aldrich, Brazil. The experiments were carried out in cylindrical glass recipients (9.0 cm of diameter and 5.5 cm high) in which 300 mL aliquots of the TBP solutions were subjected to 6 hours of exposure to a germicidal lamp UV-254 nm (Philips, 30 W). Although it is known that UVA radiation is cost-effective for the use in TiO_2 photocatalysis, the UVC photoreactor was used to assure higher degradation of the target compound. The lamps were pre-heated for 10 minutes before each treatment to stabilize the photoemissions and the samples were kept under constant stirring during the process. The photocatalytic reactor and its components are illustrated in Figure 1.

Three sets of experiments were run, first using only the germicidal lamps and then using the photocatalyst titanium dioxide (TiO_2) in suspension and supported on a cylindrical metal plate with dimensions of 17cm x 3cm (radius of 2.71 cm). The metal support was impregnated with a composite suspension of 0.30 of TiO_2/0.15 Nyacol. TiO_2 was acquired in the commercial form P25 from Evonik Degussa Brasil ltda, Brazil. 300 mg of P25 TiO_2 were used in suspension and on the support. This amount was chosen through literature review and a set of preliminary experiments carried out under the same conditions.

The room was kept under refrigeration to avoid heating in the reactor and decrease in the efficiency of the process. The temperature was measured right before and after the treatment to guarantee control of temperature. The pH was also measured before and after all the treatments. To avoid interferences in analytical measurements, after treatment with suspended TiO_2, the solution was filtered with 0.45 nm filters.

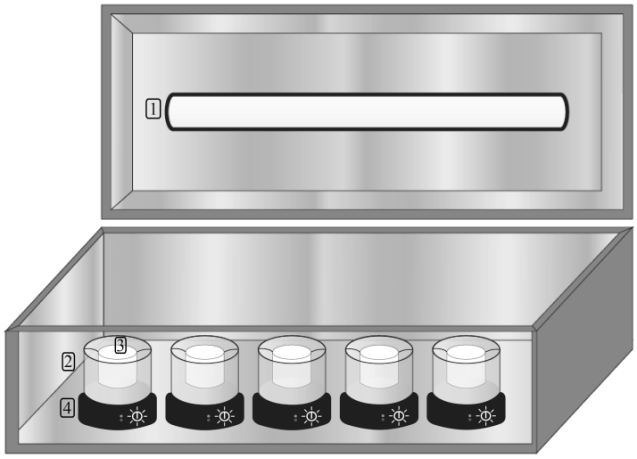

Figure 1. Photocatalytic bench reactor model. 1. Germicidal lamp (2,500 lux and 18.6 μW.cm^{-2} at 254 nm); 2. Glass reactor; 3. Metal plate with immobilized TiO_2; 4. Magnetic stirrer.

Preparation of the TiO_2 metallic support

Metal plates 17 cm long and 3 cm wide were prepared from FeCrAlloy material (72.8% iron, 22% chromium, 5% aluminum, 0.1% Yttrium and 0.1% Zirconium). The plates were previously washed with neutral detergent, acetone and distilled water before the immobilization process. After the washing procedure, the plates were weighed and heated in a muffle furnace for 24 hours under 900 °C. After cooling, each plate was weighed again for the coating procedure. For the immobilization of P25 TiO_2, a suspension consisting of 15% titanium dioxide, 30% of nyacol and 55% water acidified with nitric acid to pH 3 was prepared. The solution was placed in an UltraSonic Cleaner (Unique) for 40 minutes and subsequently stirred for 24 hours. The plates were completely immersed in the suspension for 5 minutes for each coating. After immersion, they were allowed to dry at 28 ± 2 °C. The coatings were conducted until obtaining an approximate mass of 300 mg of TiO_2. Then the plates were calcined at 450 °C for 6 hours, thus achieving a metal plate impregnated on both sides.

Characterization of the Supported Metal Plate

Scanning Electron Microscopy with Energy Dispersive X-ray Spectroscopy (SEM-EDS)

A morphologic characterization of the TiO_2 covering over the metallic substrate was obtained by SEM with a FEI microscope, model Quanta 200 FEG, available at the Nordeste Strategic Technology Center (CETENE, Brazil). The samples were prepared using approximately 1 mg of the material dispersed on a carbon tape. SEM was associated to the EDS chemical microanalysis technique to characterize the chemical surface of the plates and carry out the chemical mapping of the coating material.

X-Ray Diffraction (XRD)

XRD was used to assess the effects of the thermal treatment on the formation of crystalline phases. For this purpose, a Bruker ADVANCE 8 diffractometer available in CETENE, Brazil, was used with CuKα radiation (λ = 1.5406 Å) and 2θ ranging from 20 to 80° with a ster of 0.02º and scanning speed of 1 θ/min.

Adherence Test of Supported Metal Plate

The adherence of the photocatalytic layer deposited onto the substrate was evaluated using an ultrasonic technique (Meille et al., 2005). The weight loss caused

by the exposition of the sample to ultrasounds is measured. The plates of 2 x 2 cm dimensions immersed in petroleum ether were submitted to an ultrasonic treatment for 30 min at room temperature. After that, the samples were dried and calcined. The weight loss was determined by the difference in the mass of the samples before and after the ultrasonic test. The results are presented in terms of retained amount of coating on the plate, expressed as percentage (Table 1).

Table 1. Washcoating characteristics of the photocatalytic onto FeCrAlloy substrate.

	Initial mass adhered in the plate (mg)	Final mass after test (mg)	Adherence (%)
Plate 1	24.2	22.1	91
Plate 2	25.1	23.5	94
Plate 3	24.7	22.9	93

Analytical Procedure

The samples were analyzed by UPLC performed on an Acquity ultra performance liquid chromatography system (Waters, USA). The system was coupled to a single quadrupole SQ Detector 2 mass spectrometer (Waters, USA), equipped with an electrospray ionization analyzer in positive mode. The parameters of the ionization source: capillary voltage (kV) 3.5, cone voltage (V) 25, Desolvation temperature (°C) 150, source gas flow (L.Hr-1) 550. The analysis was determined and quantified by the Selected Ion Recording "(SIR), where the mass 266.32 g.mol-1, referring to TBP, was investigated. The observation of the degradation profile of TBP was performed in the "Full Scan" mode, with mass search in the 100-1000 Da range, using the same SIR mode source parameters.

Kinetic Modelling Through ANN

The kinetic models were established for the UVC/Plate and UVC/TiO_2 system. The ANN was developed with initial TBP concentration and the time as input variables to generate a curve of concentration over time, similarly as applied by Go et al. (1999) and Giroto et al. (2006). For this purpose, a software was created based on C# language in Unity 3D©. The ANN is composed of input, hidden and output layers with different numbers of neurons. A group of procedures was set to make the adjustment possible. The type of ANN used was 1:2:1 (1 input variable, 2 hidden layers and 1 output variable). The data used is automatically divided into regions of training, interpolation and extrapolation by the software.

The training method was based on the method Particle Swarm Optimization (PSO) (Kennedy and Eberhart, 1995) and random search (Rastrigin, 1963), in which a small disturbance was induced in the weights and biases to verify if the resultant network is a better adjustment according to the experimental data. The training lasted 316 seconds for the UVC/Plate system and 209 seconds for the UVC/TiO_2 system until reaching enough interactions for the fitting process. All trainings were performed on a regular desktop computer.

The training of simple ANN topology was tested and the result according to the mean absolute error was adopted for both UVC/Plate and UVC/TiO_2 models. A two-layer feedforward was adopted, with a sigmoid neuron-response function, and an independent (bias) term for the intermediate and output neuron layers, as described by Haikin (1999). To perform the ANN analysis the input and output values were normalized and established between -1 and 1 for all sets of data in order to guarantee the training to be reliable and rapid (Haikin, 1999). The network input used in the UVC/plate system was normalized from [0,4000] to [-1,1] and the network input for the UVC/TiO2 system was normalized from [0,2000] to [-1,1].

Toxicity Assessment Using *Artemia Salina*

The toxicity assessment was carried out for solutions before and after the treatments with 100 $\mu g.L^{-1}$. *Artemia salina* eggs were incubated in sea water, which was collected until 48 h before the assay and was kept at 25ºC, pH 7-8 and in the absence of light for 24 hours (Freitas et al., 2011; Rocha-Filho et al., 2015). The eggs were hatched after this period and then moved to Falcon tubes with 2.5 mL of natural sea water. According to the standard procedure, the samples were diluted in sea water to four different concentrations (12.5%, 25%, 50% and 100% v/v) and 5 mL were used in Falcon tubes with 10 crustaceans each.

The repeatability of the bioassay was assured by the use of at least five replicates for each concentration as observed in the literature (Freitas et al., 2011). In the negative control, larvae were only incubated in seawater, without the effluent; thus, ten *Artemias* were placed in the 5 mL of seawater (Meyer et al., 1982). After 24 hours of incubation under the same conditions, the survival rate (%) was reported and the concentration required to kill 50% (LC_{50}) of larvae was determined and the 95% confidence intervals were calculated. The acute toxicity related to the LC_{50} was calculated by the *Statistica 8.0* software.

RESULTS AND DISCUSSION

FeCrAlloy Metal Plate Characterization by SEM-EDS

Figure 2 shows the SEM analysis of the metal plate covered by P25 TiO_2. In Figure 2(a) a homogeneous coating with several cracks can be observed, probably due to the effect of the final drying temperature imposed on the sample. However, it was evidenced

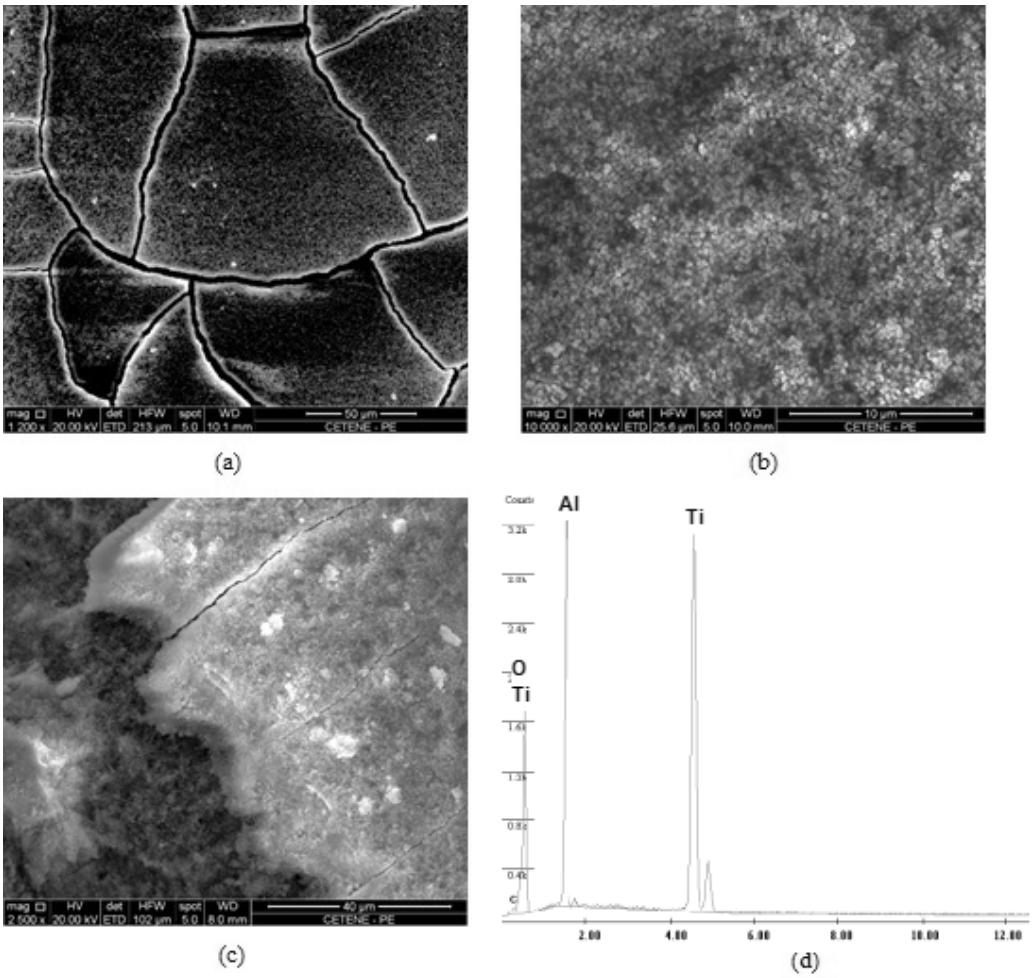

Figure 2. SEM analysis of the metal plate covered by P25 TiO_2.

by the adhesion tests that, despite the presence of this type of coating cracks, there was no leaching of substrate particles, demonstrating the effectiveness of the preparation of the suspension and coating. The cracks in the surface coating increase light absorption, since, according to the literature, the greater the roughness of the surface the less is the reflection of light and therefore the greater the absorption (Ray and Beenackers, 1998). Figure 2(b) points to a good homogeneity of TiO_2 and Al_2O_3 particles deposited on the metallic alloy. From Figure 2(c), a TiO_2 film thickness of approximately 10 μm can be estimated. Finally, in Figure 2(d), the elements Ti, O and Al were identified.

FeCrAlloy Metal Plate Characterization by XRD

The XRD spectrum of the immobilized P25 TiO_2 on the FeCrAlloy substrate is shown in Figure 3.

The qualitative interpretation of the compounds present in the catalysts was performed from the Inorganic Crystal Structure Database (ICSD): 21-1272; 21-1276; 47-1308; 1-2665. It is possible to note the presence of the anatase and rutile phases of TiO_2, as well as the presence of γ-Al_2O_3 from the suspension

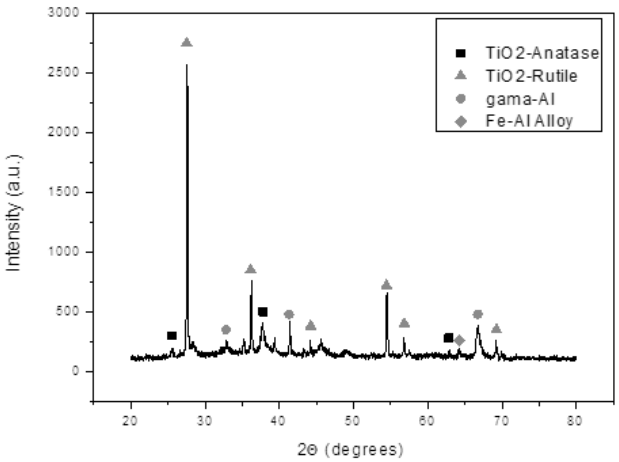

Figure 3. XRD spectrum of P25 TiO_2 supported over a FeCrAlloy metal substrate.

additive (NYACOL®-20) at 32.75°, 41.43° and 66.72°. The peaks that appear at 25.62°, 37.76° and 62.85° refer to the anatase phase of titanium oxide for different crystalline planes. The rutile phase of TiO_2 peaks appear at 27.55°, 36.22°, 44.28°, 54.48°, 56.83° and 69.28°. The peak at 64.18° probably corresponds to the presence of the Fe-Al alloy of the metal substrate.

Adherence Test of Supported Metal Plate

The excellent adhesion found, above 90%, came from the formulation of the catalytic suspension with Nyacol additive (30% of the Al_2O_3 nanoparticles added the suspension of the photocatalyst), which generated a chemical compatibility with the substrate (α-Al_2O_3), and presented a surface roughness (after the heat treatment) that allowed the catalyst particles to fit in the interior surface grooves, favoring the mechanical fixation of the photocatalyst.

Table 1 shows the triplicate results of the adhesion of the photocatalyst on the substrate.

Degradation of TBP by advanced oxidation processes

In the AOP experiments, no significant degradation was achieved for the blank tests performed in the dark, since in this case hydroxyl radicals are not formed in the absence of radiation. Figure 4 shows the data for TBP degradation by direct UV-C photolysis in the system UV-C/TiO_2 with suspended and immobilized TiO_2.

The most efficient of the systems tested with UV-C radiation was, as expected, UV-C/$TiO_{2(SUSP)}$, with 88.8% of TBP degradation at the end of the experiment (300 min). The process UV-C/$TiO_{2(IMMOB)}$ presented 60.7% of degradation. The UV-C direct photolysis was also able to partially remove TBP, achieving 27.5% of degradation.

The treatment using immobilized TiO_2 on the metal plate provided different results than those obtained using TiO_2 in suspension. These results were expected since the systems with supported TiO_2 films present a smaller surface area, lower radiation capture efficiency and higher transport resistance when compared to the powder in suspension (Shen et al., 2016). This can be explained by the effects of the metal support on the photocatalyst activity. A range of processes can occur during the photoabsorption such as charge transfer and orbital rehybridization due to the changes in the electronic structure of TiO_2. These processes, when on the surface of the plate, can promote an activity increase or selectivity for specific reactions, differing from the chemical behavior when in suspension (Nawi and Haitham, 2014; Pongthawornsakun et al., 2015). The enhancement in selectivity of AOPs represents an important tool to control the formation of harmful intermediates (State et al., 2017) since the change on the mechanisms of radical formation leads to different reaction pathways. It is known that mass transfer is much more limited in TiO_2 immobilized experiments, but the cost of separation represents a great disadvantage for the treatment feasibility (Hir et al., 2017). Thus, the results for UV-C/$TiO_{2(IMMOB)}$ can be considered satisfactory.

The thermal treatment (calcination) that can be applied to the metal generates a roughness that enhances adhesion of TiO_2 and diminishes lixiviation, as can be seen in the micrographs (Figure 2).

The UV-C/TiO_2 photochemical process is able to generate hydroxyl radicals (HO•) by exciting with radiation one electron from the Valence Band (VB) to the Conduction Band (CB), promoting the formation of a hole, written as h_{VB}^{+} (Mahmoodi et al., 2006), as shown in Equation 1. The process follows the chemical pathway described in the subsequent equations were HO• is formed from the hole (Eq. 2 and 3) and the organic compound is destroyed (Eq. 4 and 5).

$$TiO_2 + h\nu \rightarrow TiO_2\left(e_{CB}^{-} + h_{VB}^{+}\right) \quad (1)$$

$$TiO_2\left(h_{VB}^{+}\right) + H_2O \overset{0}{\rightarrow} HO\bullet + H^{+} + TiO_2 \quad (2)$$

$$TiO_2\left(h_{VB}^{+}\right) + HO^{-} \overset{3}{\rightarrow} HO\bullet_{adsorbed} + TiO_2 \quad (3)$$

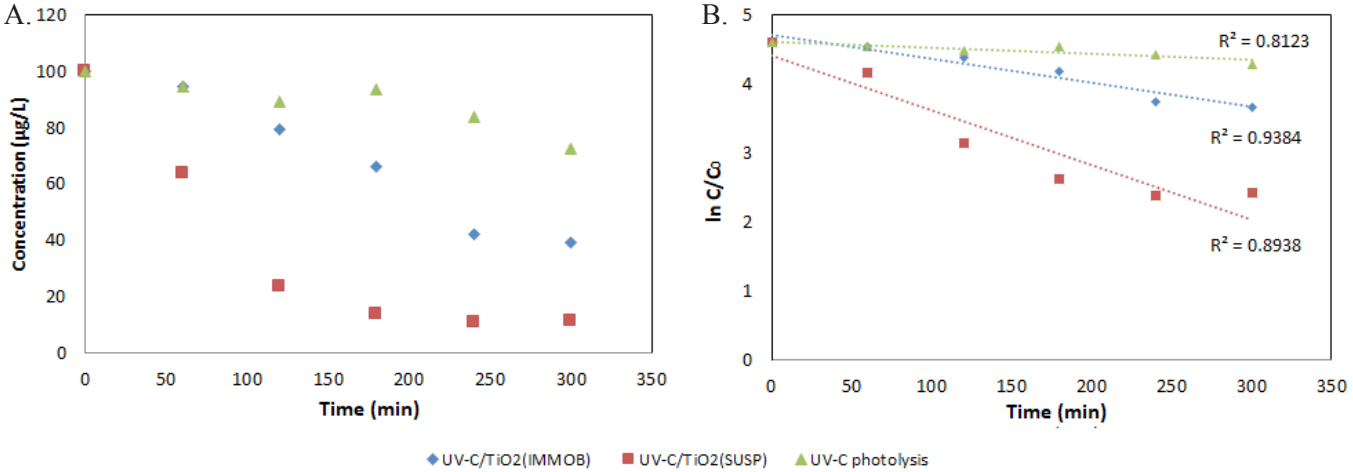

Figure 4. TBP removal profilesby UV-C photolysis, UV-C/$TiO_{2(SUSP)}$ and UV-C/$TiO_{2(IMMOB)}$ systems (a) and liner kinetic fitting to pseudo-first-order model (b).

$$HO\bullet + TBP \xrightarrow{1} \text{by products of degradation} \quad (4)$$

$$TiO_2\left(h^+_{BV}\right) + TBP \xrightarrow{2} \text{oxidation products} \quad (5)$$

Each reaction exhibits a kinetic rate constant (k, k_0, k_3, k_1 and k_2, respectively Equations 1-5). Considering that the TBP degradation is related to Equations 4 and 5, the concentration changes along time can be written as a function of the rates of these reactions:

$$\frac{d[TBP]}{dt} = -r_1 - r_2 \quad (6)$$

$$\frac{d[TBP]}{dt} = -k_1[HO\bullet][TBP] - k_2[TBP] \quad (7)$$

Since TiO_2 is in the solid state, its concentration is not considered in the equation. The radical concentration [HO•] cannot be measured due to its unstable character, so an equation in function of stable components must be found.

$$\frac{d[\bullet OH]}{dt} = k_3\left[OH^-\right] + k_0[H_2O] - k_1[HO\bullet][TBP]$$

The $[H_2O]$ concentration can be considered constant due to the excess of $[H_2O]$ during the reaction, the $[OH^-]$ concentration can be considered as zero due to its small value in comparison to the other compounds, and is quickly consumed as described in equation 3.

$$k_4 = k_3\left[OH^-\right] + k_0[H_2O]$$

$$\frac{d[\bullet OH]}{dt} + k_1[HO\bullet][TBP] = k_4$$

Applying the pseudo-steady state hypothesis to the reactive radical HO•, one obtains:

$$[HO\bullet] = \frac{k_4}{k_1[TBP]} \quad (8)$$

Replacing the expression for [HO•] in Equation 7, we obtain Equation 9.

$$\frac{d[TBP]}{dt} = -k_1\left[\frac{k_4}{k_1[TBP]}\right][TBP] - k_2[TBP]$$

$$\frac{d[TBP]}{dt} = -k_4 - k_2[TBP] \quad (9)$$

According to Equation 9, we can describe the process as a first order reaction with an added constant term, since in the fitting k4 it turned out to be orders of magnitude lower than k2. approaching a pseudo-first-order model, model which was used thereafter. using only one kinetic constant called "k".

The data for the three treatments were adjusted yet to kinetic zero-order, pseudo-first-order and second-order models by regression analysis. According to the mathematical modelling and correlation coefficients (R^2) only the pseudo-first-order model provided satisfactory results (R^2>0.80). Table 2 shows the correlation coefficents and the kinetic rate constants obtained for each system with a pseudo-first-order kinetic model fitting.The reaction half-lifes ($t_{1/2}$) were also estimated.

The kinetic adjustment is in accordance with the degradation results, showing that UV-C/$TiO_{2(SUSP)}$ is the most efficient system with larger kinetic constant and lower reaction half-life time, the time the reaction takes to remove 50% of TBP under the conditions applied. It is possible to conclude from the data in the table that the UV-C/$TiO_{2(IMMOB)}$ efficiency is aproximately 56% of the UV-C/$TiO_{2(SUSP)}$ efficiency and UV-C photolysis is only 9%.

Figure 5 displays the TBP chromatograms of the raw sample and after the treatments. The retention time was obtained at 4.38 minutes for 266.32 $g.mol^{-1}$. After the treatments (c) and (d), the generation of intermediate species with different peaks can be observed.

Kinetic Modelling Through ANN

Due to a not ideal fit for pseudo first order model, a neural network model was developed. The data was not enough to provide degrees of freedom to the training, so interpolated data was used to achieve enough data points, as exposed in the table 3. In Table 3 the points with an asterisk are interpolated points obtained by linear interpolation to complete the training set and avoid overfitting. Still in the Table 3 is possible make comparisons between the experimental data and the data calculated by the neural models.

ANN results from TBP degradation data training for the UVC/Plate are presented in Figure 6. Figure 6a shows the input layer (time of degradation) and the output layer (representing the degradation response). The weights (values above the lines connecting the neurons) indicate the values which multiply the output values of a neuron before the value gets to the next neuron, while the bias

Table 2. Kinetic fitting to pseudo-first-order models for the three AOP systems studied.

System	R^2	k (min^{-1})	$t_{1/2}$ (min)
UV-C	0.81	0.00090	770.16
UV-C/$TiO_{2(SUSP)}$	0.89	0.0080	86.64
UV-C/$TiO_{2(IMMOB)}$	0.94	0.0035	198.04

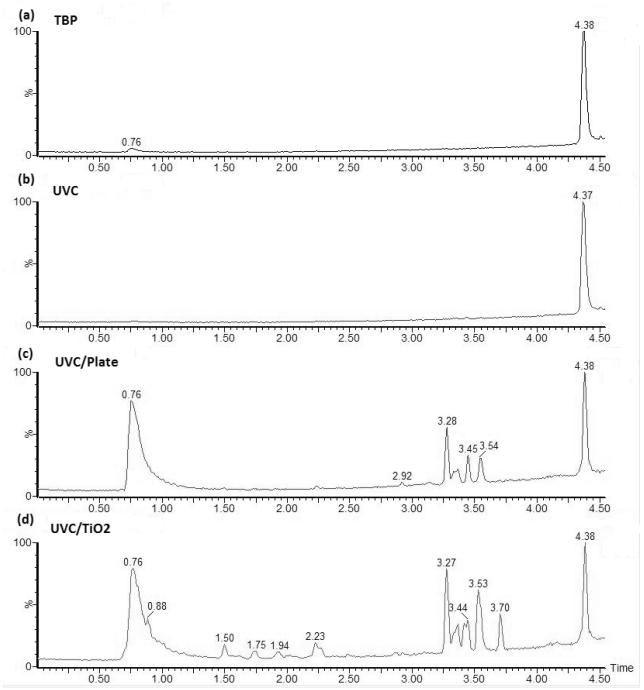

Figure 5. Chromatograms of TBP (a) raw sample, 300 minutes (b)UV-C photolysis treatment, (c) UV-C/$TiO_{2(IMMOB)}$ treatment and (d) UV-C/$TiO_{2(SUSP)}$ treatment.

(the arrows pointing to the neurons) indicate the values added to the neuron inputs. This model is able to model the degradation response for the UVC/Plate process of TBP under the given conditions.

According to the chart in Figure 6b, a good model could be achieved by the training with an absolute mean error estimated as 2.21 after 950 interactions and R^2=0.9848. It is possible to observe that the ANN model is able to interpolate the experimental points. Only the data at 240 hours could not be precisely predicted, since in Neural Networks overfitting is always avoided in order to generalize the data set. The mathematical equation that represents the network for the UVC/Plate system is Eq. 10:

$$\begin{aligned}\frac{C}{C_0} &= 2.3576\Big/\Big\{1+\exp\Big\{-\Big\{2.3097+10.3004\Big/\Big\{1+\\ &+ \exp\Big[-\big(-8.4249-8.4391\cdot t\big)\Big]\Big\}+0.2914\Big/\Big\{1+\\ &+ \exp\Big[-\big(-7.6252-9.5927\cdot t\big)\Big]\Big\}-0.1457-5.1502\Big\}\Big\}-1.1788\end{aligned} \quad (10)$$

The equation 10 is valid only for the normalized training interval t ϵ [-1,-0.85] equivalent to [0,300] hours. The ANN model derived from the TBP degradation data training for the UVC/TiO_2 system is exhibited in Figure 7.

Table 3. Data used in the network training, and results obtained.

Time (hours)	Concentration Exp. (µg/L) UVC/Plate	Concentration Neural model UVC/Plate	Concentration Exp. (µg/L) UVC/TiO_2	Concentration Neural model UVC/TiO_2
0	100	99.63	100	99.99
60	94.633	92.18	63.733	63.73
90*	87.000*	86.95	43.533*	39.81
120	79.366	80.7	23.333	25.33
150*	72.733*	73.55	18.550*	17.97
180	66.1	65.75	13.766	14.27
210*	54.10*	57.67	12.266*	12.35
240	42.1	49.68	10.766	11.31
270*	40.683*	42.12	11.000*	10.75
300	39.266	35.23	11.233	10.44

* Interpolated values used to increase the number of data for training the ANN model.

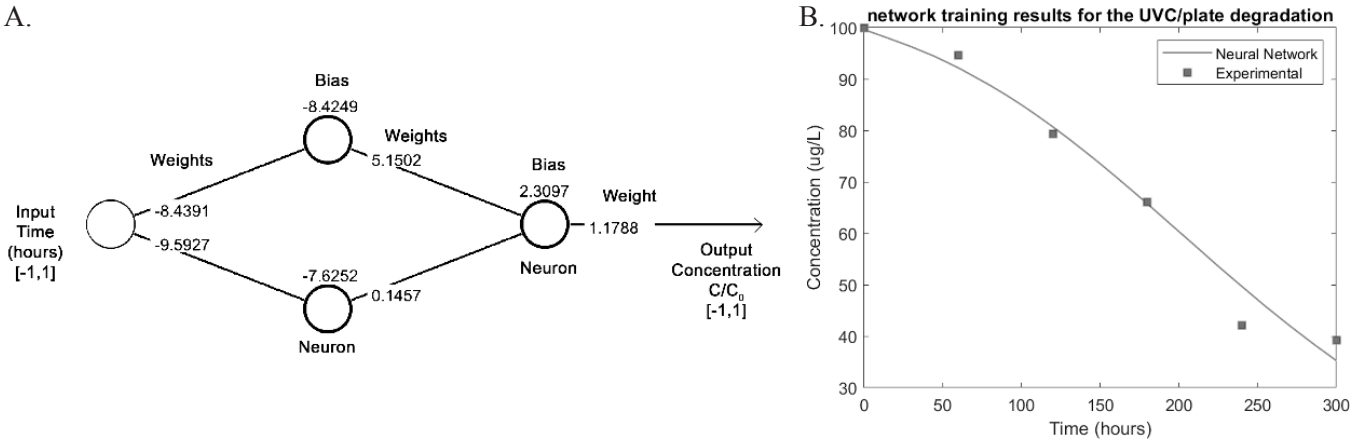

Figure 6. (a) Resulting ANN for the TBP degradation data in the UVC/Plate system. (b) Fitting of the ANN model for the UVC/Plate experimental data.

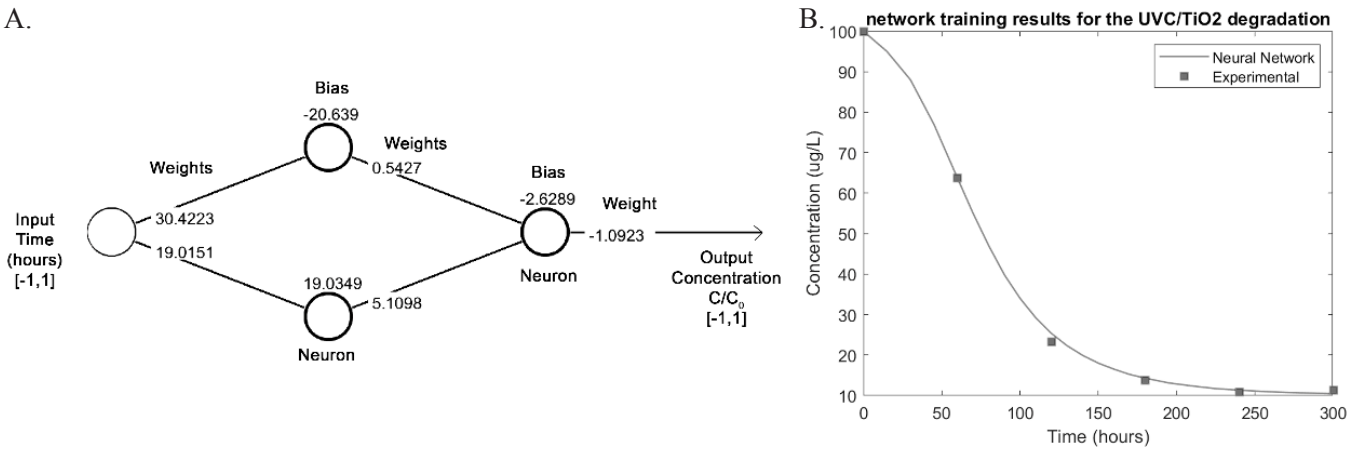

Figure 7. (a) Resulting ANN for the TBP degradation data in the UVC/TiO_2 system. (b) Fitting of the ANN model for the UVC/ TiO_2 experimental data.

The generalization of the training was also accomplished with quality for the UVC/TiO_2 experiment and the mean absolute error was estimated as 0.70 and R^2=0.9987 after 780 interactions for the photocatalytic process. These results confirm that the model reproduces the degradation of TBP, and the agreement between the model predictions and the experimental data is adequate for both situations. The mathematical equation that represents the network for the UVC/TiO_2 system is Eq. 11:

$$\frac{C}{C_0} = -2.1846\Big/\Big\{1+\exp\Big\{-\Big\{-2.6289+1.0854\Big/\{1+ + \exp\Big[-\big(-20.639+30.4223\cdot t\big)\Big]\Big\}+10.2196\Big/\{1+ + \exp\Big[-\big(19.0349+19.0151\cdot t\big)\Big]\Big\}-5.1098-0.5427\Big\}\Big\}+1.0923 \quad (11)$$

The equation 11 is valid only for the normalized training interval t ϵ [-1,-0.7] equivalent to [0,300] hours.

Toxicity Assessment Using *Artemia Salina*

Phytotoxicity bioassays were conducted in order to verify the acute toxicity of these intermediates compared to the parent compound. The results of the toxicity tests are shown in Table 4.

The treatments with heterogeneous photocatalysis using immobilized TiO_2 were able to reduce the

Table 4. Ecotoxicity tests - Summary of LC_{50} values observed for each sample ($p < 0.05$).

Sample/Status	LC_{50} value (Median ± SD)/%(v/v)
TBP before treatment	10.22 ± 0.51
TBP after direct photolysis	10.04 ± 0.87
TBP after treatment with supported TiO_2	16.89 ± 0.56
TBP after treatment with suspended TiO_2	NCR*

* NCR - Not Considerable Rates (achieved for the assays performed with TBP treated samples even at 100% concentration - pure sample).

Table 5. Studies on the degradation of OPFRs by alternative treatment methods.

OPFR	Treatment Method	Concentration ($mg.L^{-1}$)	Time	Removal (%)	Reference
TBP	Microbial degradation: free *Pseudomonas pseudoalcaligenes*	75	6 days	100	Chaudhari et al. (2012)
TBP	Microbial degradation: immobilized *Pseudomonas pseudoalcaligenes*	75	5 days	100	Chaudhari et al. (2012)
TBP	Microalgae biodegradation: *Chlorella* and *Scenedesmus sp.*	0.005	10 days	>90%	Matamoros et al. (2016)
TCEP	Microalgae biodegradation: *Chlorella* and *Scenedesmus sp.*	0.005	10 days	<20%	Matamoros et al. (2016)
TBP	Microbial degradation: aerobic granular biofilms	532.64	5 h	100	Nancharaiah et al. (2015)
Aliphatic OPFR (including TBP and TBEP)	AOP: UV/O_3	1000	-	>70%	Yuan et al. (2015)
Chlorinated OPFRs	AOP: UV/O_3	1000	-	<30%	Yuan et al. (2015)
TBP	AOP: UV-C photolysis	0.1	5 h	27.5	This work
TBP	AOP: UV-C/$TiO_{2(free)}$	0.1	5 h	88.8	This work
TBP	AOP: UV-C/$TiO_{2(immobilized)}$	0.1	5 h	60.7	This work

TBEP = tris (2-butoxyethyl) phosphate. TCEP = tris (2-butoxyethyl) phosphate.

toxicity, proving that the formation of more toxic intermediates did not occur. In the treatment using only direct photolysis, the LC_{50} value was at the same level as that obtained for the TBP solution without treatment, showing that this degradation formed intermediates with similar TBP toxicity. The treatment with suspended TiO_2 reduced toxicity to levels which were not possible to estimate the LC_{50}, pointing that they were considerably less toxic than the parent compound. No inhibitory effects were exhibited in the organisms by the treated samples with TiO_2-suspended system

Table 5 lists some reports in the literature that apply treatment technologies for the removal of OPFRs and their respective efficiency.

According to the table it is possible to observe that different technologies have achieved great efficiencies in the removal of OFPRs at high or low concentrations. Microbial treatments are normally associated with high treatment time and generation of contaminated biomass and, in some cases, are associated with complex operation. AOP treatments have shown great removal rates with feasible operational times . The advantage of TiO_2 usage relies on its nontoxic and catalytic properties, being associated with a recycling of the oxidizing agent (Ali et al., 2015). It can be also highlighted that chlorinated OFPRs usually present larger resistance to different degradation treatments.

CONCLUSIONS

According to the photocatalytic treatment results, it was possible to verify the efficacy of TBP degradation in the studied systems. As could be anticipated, the TiO_2 system supported on metal plates exhibited lower efficiency when compared to the suspended TiO_2 system. However, the results are considered good since no posterior separation step is needed in the immobilized systems and represents a great saving in operational costs and effort. The toxicity tests demonstrated that, in general, the applied treatment is adequate to reduce toxicity, except for the treatment using only direct photolysis. The metal alloy has proven to be an easy and feasible alternative for TiO_2 immobilization. The use of ANN was proven to be a promising alternative to model the degradation of TBEP by oxidation processes with low absolute errors and high determination coefficients.

ACKNOWLEDGEMENTS

The authors are grateful to Conselho Nacional de Desenvolvimento Científico e Tecnológico (CNPq) and Fundação ao Amparo e Desenvolvimento de Pernambuco (FACEPE) for the financial support.

REFERENCES

Ali, S., Firozjaei, A., Latifi, A. M., Khodi, S., Abolmaali, S. A Review on Biodegradation of Toxic Organophosphate Compounds. Journal of Applied Biotechnology Reports, 2, 215-224 (2015).

Borges, R., Alves, L., Silva, R. J. C., Araújo, M. F., Candeias, A., Corregidor, V., Valério, P., Barrulas, P. Investigation of surface silver enrichment in ancient high silver alloys by PIXE, EDXRF, LA-ICP-MS and SEM-EDS. Microchemical Journal, 131, 103-111 (2017). https://doi.org/10.1016/j.microc.2016.12.002

Cheng, M., Zeng, G., Huang, D., Lai, C., Xu, P., Zhang, C., Liu, Y., Hydroxyl radicals based advanced oxidation processes (AOPs) for remediation of soils contaminated with organic compounds: A review. Chemical Engineering Journal, 284, 582-598(2016). https://doi.org/10.1016/j.cej.2015.09.001

Cristale, J., Ramos, D. D., Dantas, R. F., Machulek Junior, A., Lacorte, S., Sans, C., Esplugas, S. Can activated sludge treatments and advanced oxidation processes remove organophosphorus flame retardants?. Environmental Research, 144, 11-18 (2016). https://doi.org/10.1016/j.envres.2015.10.008

Dai, H., Sun, Y., Ni, P., Lu, W., Jiang, S., Wang, Y., Li, Z., Li, Z. Sensors and Actuators B : Chemical Three-dimensional TiO_2 supported silver nanoparticles as sensitive and UV-cleanable substrate for surface enhanced Raman scattering. Sensors & Actuators: B. Chemical, 242, 260-268 (2017). https://doi.org/10.1016/j.snb.2016.10.085

De la Cruz, N., Esquius, L., Grandjean, D., Magnet, A., Tungler, A., de Alencastro, L. F., Pulgarín, C. Degradation of emergent contaminants by UV, UV/H2O2 and neutral photo-Fenton at pilot scale in a domestic wastewater treatment plant. Water Research, 47, 5836-5845 (2013). https://doi.org/10.1016/j.watres.2013.07.005

de Wit, C. A., Herzke, D., Vorkamp, K. Brominated flame retardants in the Arctic environment - trends and new candidates. Science of the Total Environment, 408, 2885-2918 (2010). https://doi.org/10.1016/j.scitotenv.2009.08.037

El Fels, L., Hafidi, M., Ouhdouch, Y. Artemia salina as a new index for assessment of acute cytotoxicity during co-composting of sewage sludge and lignocellulose waste. Waste Management, 50, 194-200 (2016). https://doi.org/10.1016/j.wasman.2016.02.002

Estévez, E., Cabrera, M. del C., Molina-Díaz, A., Robles-Molina, J., Palacios-Díaz, M. del P. Screening of emerging contaminants and priority substances (2008/105/EC) in reclaimed water for

irrigation and groundwater in a volcanic aquifer (Gran Canaria, Canary Islands, Spain). Science of the Total Environment, 433, 538-546 (2012). https://doi.org/10.1016/j.scitotenv.2012.06.031

Flaskos, J. The developmental neurotoxicity of organophosphorus insecticides: A direct role for the oxon metabolites. Toxicology Letters, 209, 86-93 (2012). https://doi.org/10.1016/j.toxlet.2011.11.026

Focazio, M. J., Kolpin, D. W., Barnes, K. K., Furlong, E. T., Meyer, M. T., Zaugg, S. D., Barber, L.B., Thurman, M. E. A national reconnaissance for pharmaceuticals and other organic wastewater contaminants in the United States - II) Untreated drinking water sources. Science of the Total Environment, 402, 201-216 (2008). https://doi.org/10.1016/j.scitotenv.2008.02.021

Freitas, M. C. R., António, J. M. S., Ziolli, R. L., Yoshida, M. I., Rey, N. A., Diniz, R., Synthesis and structural characterization of a zinc(II) complex of the mycobactericidal drug isoniazid - Toxicity against Artemia salina. Polyhedron, 30, 1922-1926 (2011). https://doi.org/10.1016/j.poly.2011.04.027

Giannakis, S., Gamarra Vives, F. A., Grandjean, D., Magnet, A., De Alencastro, L. F., Pulgarin, C. Effect of advanced oxidation processes on the micropollutants and the effluent organic matter contained in municipal wastewater previously treated by three different secondary methods. Water Research, 84, 295-306 (2015). https://doi.org/10.1016/j.watres.2015.07.030

Giroto, J. A., Guardani, R., Teixeira, A. C. S. C., Nascimento, C. A. O. Study on the photo-Fenton degradation of polyvinyl alcohol in aqueous solution. Chemical Engineering and Processing, 45, 523-532 (2006). https://doi.org/10.1016/j.cep.2005.12.001

Go, S., Oliveros, E., Bossmann, S. H., Guardani, R., Nascimento, C. A. O. Modeling the kinetics of a photochemical water treatment process by means of artificial neural networks. Chemical Engineering and Processing, 38, 373-382 (1999). https://doi.org/10.1016/S0255-2701(99)00028-8

Haikin, S. Neural Networks: A Comprehensive Foundation (second). Upper Saddle River: Prentice Hall (1999).

Hir, Z. A. M., Moradihamedani, P., Abdullah, A. H., Mohamed, M. A. Immobilization of TiO_2 into polyethersulfone matrix as hybrid film photocatalyst for effective degradation of methyl orange dye. Materials Science in Semiconductor Processing, 57, 157-165 (2017). https://doi.org/10.1016/j.mssp.2016.10.009

Hsieh, B. J., Tsai, M. C., Pan, C. J., Su, W. N., Rick, J., Chou, H. L., Lee, J. R., Hwang, B. J. Tuning metal support interactions enhances the activity and durability of TiO2-supported Pt nanocatalysts. Electrochimica Acta, 224, 452-459 (2017). https://doi.org/10.1016/j.electacta.2016.12.020

Jung, H., Park, E., Kim, M., Jurng, J. Pilot-scale evaluation of a novel TiO_2-supported V2O5 catalyst for DeNOx at low temperatures at a waste incinerator. Waste Management, 61, 283-287 (2017). https://doi.org/10.1016/j.wasman.2016.11.006

Karci, A., Arslan-Alaton, I., Bekbolet, M. Advanced oxidation of a commercially important nonionic surfactant: Investigation of degradation products and toxicity. Journal of Hazardous Materials, 263, 275-282 (2013). https://doi.org/10.1016/j.jhazmat.2013.03.052

Kennedy, J., Eberhart, R. Particle swarm optimization. In IEEE International Conference (1995).

Klavarioti, M., Mantzavinos, D., Kassinos, D. Removal of residual pharmaceuticals from aqueous systems by advanced oxidation processes. Environment International, 35, 402-417 (2009). https://doi.org/10.1016/j.envint.2008.07.009

Krivoshiev, B. V., Dardenne, F., Blust, R., Covaci, A., Husson, S. J. Elucidating toxicological mechanisms of current flame retardants using a bacterial gene profiling assay. Toxicology in Vitro, 29, 2124-2132 (2015). https://doi.org/10.1016/j.tiv.2015.09.001

Libralato, G., Prato, E., Migliore, L., Cicero, A. M., Manfra, L. A review of toxicity testing protocols and endpoints with Artemia spp. Ecological Indicators, 69, 35-49 (2016). https://doi.org/10.1016/j.ecolind.2016.04.017

Liu, X., Ji, K., Jo, A., Moon, H. B., Choi, K. Effects of TDCPP or TPP on gene transcriptions and hormones of HPG axis, and their consequences on reproduction in adult zebrafish (Danio rerio). Aquatic Toxicology, 134-135, 104-111 (2013). https://doi.org/10.1016/j.aquatox.2013.03.013

Lo Nostro, P., Ninham, B. W., Carretti, E., Dei, L., Baglioni, P. Specific anion effects in Artemia salina. Chemosphere, 135, 335-340 (2015). https://doi.org/10.1016/j.chemosphere.2015.04.080

Mahmoodi, N. M., Arami, M., Limaee, N. Y., Tabrizi, N. S. Kinetics of heterogeneous photocatalytic degradation of reactive dyes in an immobilized TiO_2 photocatalytic reactor. Journal of Colloid and Interface Science, 295, 159-164 (2006). https://doi.org/10.1016/j.jcis.2005.08.007

Matamoros, V., Uggetti, E., García, J., Bayona, J. M. Assessment of the mechanisms involved in the removal of emerging contaminants by microalgae from wastewater : a laboratory scale study. Journal of Hazardous Materials, 301, 197-205 (2016). https://doi.org/10.1016/j.jhazmat.2015.08.050

Matilainen, A., Sillanpää, M. Removal of natural organic matter from drinking water by advanced oxidation processes. Chemosphere, 80, 351-365 (2010). https://doi.org/10.1016/j.chemosphere.2010.04.067

Meille, V., Pallier, S., Santa Cruz Bustamante, G. V., Roumanie, M., Reymond, J. P. Deposition of γ-Al_2O_3 layers on structured supports for the design of new catalytic reactors. Applied Catalysis A: General, 286, 232-238 (2005). https://doi.org/10.1016/j.apcata.2005.03.028

Meyer, B., Ferrigni, N. R., Putnam, J. E., Jacobsen, L. B., Nichols, D. E., McLaughlin, J. L. Brine Shrimp: A Convinient General Bioassay for Active Plant Consyituents. Journal of Medicinal Plant Research, 45, 31-34 (1982).

Nancharaiah, Y. V, Reddy, G. K. K., Mohan, T. V. K., Venugopalan, V. P. Biodegradation of tributyl phosphate , an organosphate triester , by aerobic granular biofilms. Journal of Hazardous Materials, 283, 705-711 (2015). https://doi.org/10.1016/j.jhazmat.2014.09.065

Nawi, R. M. A., Haitham, K. Fabrication, characterization and application of a reusableimmobilized TiO_2-PANI photocatalyst plate for the removal ofreactive red 4 dyeS. Applied Surface Science, 319, 90-98 (2014). https://doi.org/10.1016/j.apsusc.2014.07.049

Oller, I., Malato, S., Sánchez-Pérez, J. A. Combination of Advanced Oxidation Processes and biological treatments for wastewater decontamination-A review. Science of the Total Environment, 409, 4141-4166 (2011). https://doi.org/10.1016/j.scitotenv.2010.08.061

Ouyang, L., Liu, Q., Xu, C., Liu, C., Liang, H. Powder X-ray diffraction detection on a paper-based platform. Talanta, 164, 283-290 (2017). https://doi.org/10.1016/j.talanta.2016.11.021

Pongthawornsakun, B., Mekasuwandumrong, O., Prakash, S., Ehret, E., Santos Aires, F. J. C., Panpranot, J. Effect of reduction temperature on the characteristics and catalytic properties of TiO_2 supported AuPd alloy particles prepared by one-step flame spray pyrolysis in the selective hydrogenation of 1-heptyne. Applied Catalysis A: General, 506, 278-287 (2015). https://doi.org/10.1016/j.apcata.2015.09.012

Rastrigin, L.A. The convergence of the random search method in the extremal control of a many parameter system. Automation and Remote Control, 24, 1337-1342. (1963)

Ray, A. K., Beenackers, A. A. C. M. Development of a new photocatalytic reactor for water purifcation. Catalysis Today, 40, 73-83 (1998). https://doi.org/10.1016/S0920-5861(97)00123-5

Rocha-Filho, C. A. A., Albuquerque, L. P., Silva, L. R. S., Silva, P. C. B., Coelho, L. C. B. B., Navarro, D. M. A. F., Albuquerque, M. C. P. A., Melo, A. M. M. A., Napoleão, T. H., Pontual, E. V., Paiva, P. M. G. Assessment of toxicity of Moringa oleifera flower extract to Biomphalaria glabrata, Schistosoma mansoni and Artemia salina. Chemosphere, 132, 188-192 (2015). https://doi.org/10.1016/j.chemosphere.2015.03.041

Sagar, J. T., Burgess, S. R., McCarthy, C., Li, X. Elemental characterisation of sub 20 nm structures in devices using new SEM-EDS technology. Microelectronics Reliability, 64, 367-369 (2016). https://doi.org/10.1016/j.microrel.2016.07.080

Sanusi, S. N. A., Halmi, M. I. E., Abdullah, S. R. S., Hassan, H. A., Hamzah, F. M., Idris, M. Comparative process optimization of pilot-scale total petroleum hydrocarbon (TPH) degradation by Paspalum scrobiculatum L. Hack using response surface methodology (RSM) and artificial neural networks (ANNs). Ecological Engineering, 97, 524-534 (2016). https://doi.org/10.1016/j.ecoleng.2016.10.044

Shen, Y., Wang, W., Xiao, K. Synthesis of three-dimensional carbon felt supported TiO2 monoliths for photocatalytic degradation of methyl orange. Journal of Environmental Chemical Engineering, 4, 1259-1266 (2016). https://doi.org/10.1016/j.jece.2016.01.026

State, R., Papa, F., Tabakova, T., Atkinson, I., Negrila, C. and Balint, I., Photocatalytic abatement of trichlorethylene over Au and Pd-Au supported on TiO2 by combined photomineralization/hydrodechlorination reactions under simulated solar irradiation. Journal of Catalysis, 346, 101-108 (2017). https://doi.org/10.1016/j.jcat.2016.11.032

Wang, L., Wang, X., Yin, J., Zhu, Y., Wang, C. Silica induced oxygen vacancies in supported mixed-phase TiO2 for photocatalytic degradation of phenol under visible light irradiation. Catalysis Communications, 87, 98-101 (2016). https://doi.org/10.1016/j.catcom.2016.09.011

Willumeit, R., Feyerabend, F., Huber, N. Acta Biomaterialia Magnesium degradation as determined by artificial neural networks q. Acta Biomaterialia, 9, 8722-8729 (2013). https://doi.org/10.1016/j.actbio.2013.02.042

Yuan, X., Lacorte, S., Cristale, J., Dantas, R. F., Sans, C., Esplugas, S., Qiang, Z. Removal of organophosphate esters from municipal secondary effluent by ozone and UV / H_2O_2 treatments. Separation and Purification Technology, 156, 1028-1034 (2015). https://doi.org/10.1016/j.seppur.2015.09.052